Magnetotransport in a two-dimensional electron gas in the presence of spin-orbit interaction

X. F. Wang and P. Vasilopoulos
Department of Physics Concordia University, Montreal, QC H3G 1M8, Canada
(Received 19 August 2002; revised manuscript received 25 October 2002; published 26 February 2003)

We evaluate the transport coefficients of a two-dimensional electron gas in the presence of a perpendicular magnetic field and of the spin-orbit interaction (SOI) described only by the Rashba term of strength α. The SOI mixes the spin-up and spin-down states of neighboring Landau levels into two new, unequally spaced energy branches. The broadened density of states, as a function of the energy, and the longitudinal resistivity, as a function of the magnetic field, show beating patterns in agreement with observations. The positions of any two successive nodes in the beating pattern approximately determine the strength of the Rashba term. A strong SOI results in a splitting of the magnetoresistance peaks and a doubling of the number of the Hall plateaus. Each peak in the derivative of the Hall resistivity with respect to the magnetic field for $\alpha=0$ splits, for $\alpha\neq 0$, into two peaks, whose separation ΔB increases initially with α and saturates for large α.

DOI: 10.1103/PhysRevB.67.085313 PACS number(s): 73.20.At, 73.43.Qt, 72.25.Dc, 73.61.−r

I. INTRODUCTION

There has been an increasing interest in zero-magnetic-field spin splitting in one-dimensional (1D) and 2D electron systems (2DES) due to the spin-orbit interaction (SOI). Such systems have potential applications in spin-based transistors[1,2] expected to service in the future quantum computation. The SOI has been found also important in an unexpected metal-to-insulator transition in 2D (Ref. 3) hole gas, in spin-resolved ballistic transport,[4] in Aharonov-Bohm (AB) experiments,[5] and in a spin-galvanic effect.[6] The analysis of the Shubnikov–de Haas (SdH) oscillations in magnetoresistance measurements has become the main method of measuring the SOI strength in such systems.

Decades ago theoretical studies[7,8] in 3D semiconductors found that the spin degeneracy should be lifted in inversely asymmetric crystals due to the internal crystal field. Later, magnetotransport and cyclotron resonance measurements in a 2D hole system, in a modulation-doped GaAs/AlGaAs heterojunction, showed[9] evidence of zero-magnetic-field spin splitting for carriers with finite momentum. Similar experiments on 2D electron gases, formed in a GaAs/AlGaAs inversion layer, led to similar conclusions.[10] The first explanation was proposed by Bychkov and Rashba[11] employing the Rashba spin-orbit Hamiltonian, where the spin of finite-momentum electrons feels a magnetic field perpendicular to the electron momentum in the inversion plane. Though nonparabolicity of the bulk band structure of GaAs/AlGaAs could also explain the previous experimental results and bulk inversion-asymmetry induced spin splitting, at $B=0$, could dominate in heterostructures of wide-gap semiconductors, the Rashba SOI has been considered the most appropriate reason for the observation of the zero-field spin splitting in low-dimensional electron systems, especially in narrow-gap semiconductors.[12] Later, Luo *et al.*[13] investigated the SdH oscillations in a series of GaSb/InAs quantum wells and concluded that the lifting of the spin degeneracy results from the inversion asymmetry of the structure which invokes an electric field perpendicular to the layer. Using the Rashba SOI, they fit the experimental results and determined the Rashba parameter α, which describes the strength of the SOI. At the same time they concluded that contributions to the SOI from the bulk $\sim k^3$ term due to a crystal inversion asymmetry are of minor importance.

Generally, the contributions to the spin splitting in the conduction band of asymmetric heterostructures result from the bulk $\sim k^3$ term due to a crystal inversion asymmetry and from the Rashba $\sim k$ asymmetry. Due to their different momentum dependence, the former dominates in *wide-gap* structures with small thickness whereas the later dominates in *narrow-gap* structures. It was shown[14] that the k^3 term leads to anomalous beating patterns while the Rashba term leads to the regular beating patterns in magneto oscillations. Recently, the well-developed shaping technique in nanostructures has been used to control the SOI strength in 2D systems of different materials,[15–21] and principally the SdH oscillations are used to measure the Rashba parameter α.[22] However, to our knowledge there are no detailed theoretical treatments of the influence of the SOI on magnetotransport in 2D systems. We therefore aim at developing a more realistic model to describe theoretically magnetotransport in systems with SOI, in which the Rashba term dominates, and determine more accurately the parameter α.

In Sec. II we present the energy spectrum and the density of states (DOS). In Sec. III we present the results for the transport coefficients and in Sec. IV concluding remarks. Some auxiliary results are found in the Appendix.

II. EIGENVECTORS, EIGENVALUES, AND DENSITY OF STATES

We consider a 2DES in the $(x-y)$ plane and a magnetic field along the z direction. In the Landau gauge $\mathbf{A}=(-By,0,0)$ the one-electron Hamiltonian including the Rashba term reads

$$H=\frac{(\mathbf{p}+e\mathbf{A})^2}{2m^*}+\frac{\alpha}{\hbar}[\boldsymbol{\sigma}\times(\mathbf{p}+e\mathbf{A})]_z+g\mu_B B\sigma_z, \qquad (1)$$

where $\mathbf{p}$ is the momentum operator of the electrons, m^* is the effective electron mass, g the Zeeman factor, μ_B the Bohr magneton, $\boldsymbol{\sigma}=(\sigma_x,\sigma_y,\sigma_z)$ the Pauli spin matrix, and α the strength of the SOI.

Using the Landau wave functions without SOI as a basis, we can express the new eigenfunction in the form [k_x commutes with the Hamiltonian (1)]

$$\Psi_{k_x}(\mathbf{r}) = e^{ik_x x}\sum_{n,\sigma} \phi_n(y-y_c)C_n^{\sigma}|\sigma\rangle \Big/ \sqrt{L_x}$$

$$= e^{ik_x x}\sum_{n} \phi_n(y-y_c)\begin{pmatrix} C_n^{+} \\ C_n^{-} \end{pmatrix} \Big/ \sqrt{L_x}, \quad n=0,1,2,\ldots . \tag{2}$$

Here L_x is the length of the system along the x direction, $\phi_n(y-y_c)=e^{-(y-y_c)^2/(2l_c^2)}H_n[(y-y_c)/l_c]/\sqrt{\sqrt{\pi}2^n n! l_c}$ is the usual harmonic oscillator function, $\omega_c=eB/m^*$ the cyclotron frequency, $l_c=(\hbar/m^*\omega_c)^{1/2}$ the radius of the cyclotron orbit centered at $y_c=l_c^2 k_x$, n the Landau-level index, and $|\sigma\rangle$ the electron spin written as the column vector $|\sigma\rangle=\binom{1}{0}$ if it is pointing up and $\binom{0}{1}$ if it is pointing down. Substituting Eq. (2) in the Schrödinger equation $H\Psi=E\Psi$, multiplying both sides by $\phi_l(y-y_c)$, and integrating over y we obtain the following system of equations ($E_{\pm}=\pm g\mu_B B-E$)

$$\left\{ \begin{array}{c} i(\alpha/l_c)\sqrt{2l}C_{l-1}^{+}+[(l+1/2)\hbar\omega_c+E_-]C_l^{-}=0 \\ \\ [(l+1/2)\hbar\omega_c+E_+]C_l^{+}-i(\alpha/l_c)\sqrt{2(l+1)}C_{l+1}^{-}=0 \end{array} \right\},$$

$$l=0,1,2,\ldots . \tag{3}$$

This infinite system of equations is solved exactly after decomposing it into independent one- or two-dimensional secular equations. Denoting the new subband index by s we obtain

$$[1/2\hbar\omega_c+E_-]C_s^{-}=0, \quad s=0, \tag{4}$$

$$\begin{bmatrix} (s-1/2)\hbar\omega_c+E_+ & -i(\alpha/l_c)\sqrt{2s} \\ i(\alpha/l_c)\sqrt{2s} & (s+1/2)\hbar\omega_c+E_- \end{bmatrix}\begin{pmatrix} C_{s-1}^{+} \\ C_s^{-} \end{pmatrix}=0,$$

$$s=1,2,3,\ldots . \tag{5}$$

Corresponding to $s=0$, there is one level, the same as the lowest Landau level without SOI, with energy $E_0^{+}=E_0=1/2\hbar\omega_c-g\mu_B B$ and wave function $\Psi_0^{+}(k_x)=(e^{ik_x x}/\sqrt{L_x})\phi_0(y-y_c)\binom{0}{1}$. Corresponding to $s=1,2,3,\cdots$, we find two branches of levels with energies

$$E_s^{\pm}=s\hbar\omega_c\pm[E_0^2+2s\alpha^2/l_c^2]^{1/2}. \tag{6}$$

The $+$ branch is described by the wave function

$$\Psi_s^{+}(k_x)=\frac{1}{\sqrt{L_x\mathcal{A}_s}}e^{ik_x x}\begin{pmatrix} -i\mathcal{D}_s\phi_{s-1}(y-y_c) \\ \phi_s(y-y_c) \end{pmatrix}, \tag{7}$$

and the $-$ one by

$$\Psi_s^{-}(k_x)=\frac{1}{\sqrt{L_x\mathcal{A}_s}}e^{ik_x x}\begin{pmatrix} \phi_{s-1}(y-y_c) \\ -i\mathcal{D}_s\phi_s(y-y_c) \end{pmatrix}, \tag{8}$$

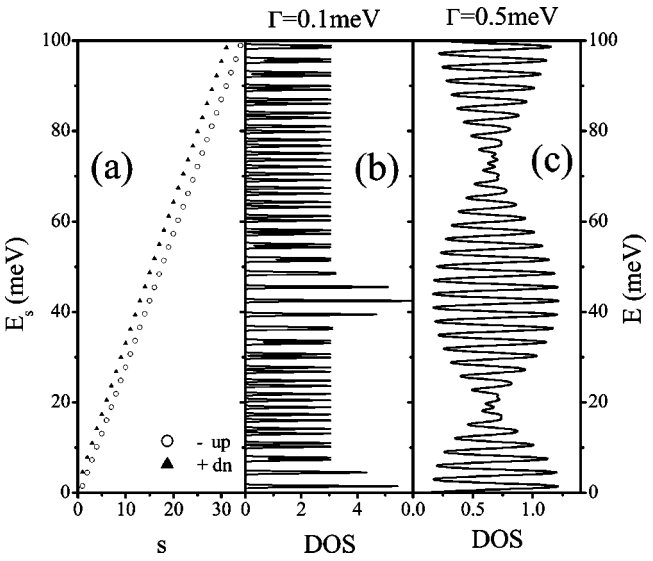

FIG. 1. (a) Subband energy E_s versus index s. The triangles are for the $+$ branch and the circles for the $-$ branch. (b) Energy (right scale) versus DOS with a subband broadening $\Gamma=0.1$ meV. (c) The same as in (b) but with $\Gamma=0.5$ meV. The other parameters are $g=2$, $B=1$ T, $m^*=0.05$, and $\alpha=10^{-11}$ eV m.

where $\mathcal{A}_s=1+\mathcal{D}_s^2$ and

$$\mathcal{D}_s=\frac{\sqrt{2s}\alpha/l_c}{E_0+\sqrt{E_0^2+2s\alpha^2/l_c^2}}. \tag{9}$$

The density of states (DOS) is defined by $D(E)=\Sigma_{sk_x\sigma}\delta(E-E_s^{\sigma})$. Assuming a Gaussian broadening of width Γ we obtain

$$D(E)=\frac{S_0}{(2\pi)^{3/2}}\sum_{s\sigma}\frac{e^{-(E-E_s^{\sigma})^2/2\Gamma^2}}{l_c^2\Gamma} \tag{10}$$

In Fig. 1(a) we plot the level energies E_s^{+} and E_s^{-} as functions of the level index s. For the case studied here we have $E_1^{-}\simeq E_0^{+}$. Because the level spacing of the $+$ branch is larger than that of the $-$ branch, the level energy of the $+$ branch increases faster and the line through the triangles (not shown) has a slope larger than that through the circles (not shown) in Fig. 1(a). Here we also notice that $E_7^{-}\simeq(E_5^{+}+E_6^{+})/2$, $E_{15}^{-}\simeq E_{13}^{+}$, $E_{25}^{-}\simeq(E_{22}^{+}+E_{23}^{+})/2$. This difference in level spacing results directly in the modulation of the density of states as shown in Figs. 1(b) and 1(c). As Fig. 1(b) shows, where the level broadening is small, $\Gamma=0.1$ meV, the DOS as a function of the energy shows peaks of the same height except when levels of different branches have the same value and higher DOS peaks appear. For wider level broadening, as shown in Fig. 1(c), with $\Gamma=0.5$ meV, the DOS is modulated and shows a beating pattern. The nodes of this pattern appear when a $-$ branch level is located near the middle between two $+$ branch levels; thus, the first node appears near the E_7^{-} level and the second node near the E_{25}^{-} one. The maximum oscillation amplitude appears when two levels of different branches are degenerate, e.g., at $E_{15}^{-}\simeq E_{13}^{+}$ here.

III. TRANSPORT COEFFICIENTS

A. Analytic results

For weak electric fields E_ν, i.e., for linear responses, and weak scattering potentials the expressions for the direct current (dc) conductivity tensor $\sigma_{\mu\nu}$, in the one-electron approximation, reviewed in Ref. 23, reads $\sigma_{\mu\nu}=\sigma^d_{\mu\nu}+\sigma^{nd}_{\mu\nu}$ with $\mu,\nu=x,y,z$. The terms $\sigma^d_{\mu\nu}$ and $\sigma^{nd}_{\mu\nu}$ stem from the diagonal and nondiagonal part of the density operator $\hat{\rho}$, respectively, in a given basis and $\langle J_\mu\rangle=\mathrm{Tr}(\hat{\rho}J_\mu)=\sigma_{\mu\nu}E_\nu$. In general, we have $\sigma^d_{\mu\nu}=\sigma^{\mathrm{dif}}_{\mu\nu}+\sigma^{\mathrm{col}}_{\mu\nu}$. The term $\sigma^{\mathrm{dif}}_{\mu\nu}$ describes the diffusive motion of electrons and the term $\sigma^{\mathrm{col}}_{\mu\nu}$ collision contributions or hopping. The former is given by

$$\sigma^{\mathrm{dif}}_{\mu\nu}=\frac{\beta e^2}{S_0}\sum_\zeta f(E^\sigma_s)[1-f(E^\sigma_s)]\tau^\zeta(E^\sigma_s)v^\zeta_\mu v^\zeta_\nu, \quad (11)$$

where $\zeta\equiv(s,\sigma,k_x)$ denotes the quantum numbers, $v^\zeta_\mu=\langle\zeta|v_\mu|\zeta\rangle$ is the diagonal element of the velocity operator v_μ, and $f(\varepsilon)$ the Fermi-Dirac function. Further, $\tau^\zeta(E^\sigma_s)$ is the relaxation time for elastic scattering, $\beta=1/k_BT$, and S_0 is the area of the system. The term $\sigma^{\mathrm{col}}_{\mu\nu}$ can be written in the form

$$\sigma^{\mathrm{col}}_{yy}=\frac{\beta e^2}{S_0}\sum_{\zeta,\zeta'}\int_{-\infty}^{\infty}d\varepsilon\int_{-\infty}^{\infty}d\varepsilon'\,\delta[\varepsilon-E^\sigma_s(k_x)]\times\delta[\varepsilon'-E^{\sigma'}_{s'}(k'_x)]f(\varepsilon)[1-f(\varepsilon')]\times W_{\zeta\zeta'}(\varepsilon,\varepsilon')(y_\zeta-y_{\zeta'})^2, \quad (12)$$

where $y_\zeta=\langle\zeta|y|\zeta\rangle$; $W_{\zeta\zeta'}(\varepsilon,\varepsilon')$ is the transition rate. For elastic scattering by dilute impurities, of density N_I, we have

$$W_{\zeta\zeta'}(\varepsilon,\varepsilon')=\frac{2\pi N_I}{\hbar S_0}\sum_{\mathbf{q}}|U(\mathbf{q})|^2|F_{\zeta\zeta'}(u)|^2\times\delta(\varepsilon-\varepsilon')\,\delta_{k_x,k'_x-q_x}, \quad (13)$$

where $u=l_c^2q^2/2$ and $q^2=q_x^2+q_y^2$. $U(\mathbf{q})$ is the Fourier transform of the screened impurity potential $U(\mathbf{r})=(e^2/4\pi\epsilon_0\epsilon)e^{-k_sr}/r$, where ϵ is the static dielectric constant, ϵ_0 the dielectric permittivity, and k_s the screening wave vector:

$$U(\mathbf{q})=\frac{e^2}{2\epsilon_0\epsilon}\frac{1}{(2u/l_c^2+k_s^2)^{1/2}}. \quad (14)$$

In the situation studied here the diffusion contribution given by Eq. (11) vanishes because the diagonal elements of the velocity operator v^ζ_μ vanish. Neglecting Landau-level mixing, i.e., taking $s'=s$, and noting that $\sigma^{\mathrm{col}}_{xx}=\sigma^{\mathrm{col}}_{yy}$, $\Sigma_{\mathbf{q}}=(S_0/2\pi)\int_0^\infty q\,dq=(S_0/2\pi l_c^2)\int_0^\infty du$, and $\Sigma_{k_x}=(S_0/2\pi l_c^2)$, we obtain

$$\sigma^{\mathrm{col}}_{yy}=\frac{N_I\beta e^2}{2\pi\hbar l_c^2}\sum_{s\sigma}\int_0^\infty du\int_{-\infty}^{\infty}d\varepsilon[\delta(\varepsilon-E^\sigma_s)]^2f(\varepsilon)\times[1-f(\varepsilon)]|U(\sqrt{2u/l_c^2})|^2|F^\sigma_{ss}(u)|^2u, \quad (15)$$

where

$$|F^-_{ss}(u)|^2=\{L_{s-1}(u)+\mathcal{D}_s^2L_s(u)\}^2e^{-u}/\mathcal{A}_s^2,$$

$$|F^+_{ss}(u)|^2=\{\mathcal{D}_s^2L_{s-1}(u)+L_s(u)\}^2e^{-u}/\mathcal{A}_s^2.$$

The exponential e^{-u} favors small values of u. Assuming $b=k_s^2l_c^2/2\gg u$,[24] we may neglect the term $2u/l_c^2$ in the denominator of Eq. (14) and obtain

$$\sigma^{\mathrm{col}}_{yy}=\frac{N_I\beta e^2}{4\pi\hbar b}\left[\frac{e^2}{2\epsilon\epsilon_0}\right]^2\sum_{s\sigma}\int_{-\infty}^{\infty}d\varepsilon[\delta(\varepsilon-E^\sigma_s)]^2f(\varepsilon)\times[1-f(\varepsilon)]I^\sigma_s, \quad (16)$$

where

$$I^\pm_s=[(2s\pm1)\mathcal{D}_s^4-2s\mathcal{D}_s^2+2s\pm1]/\mathcal{A}_s^2. \quad (17)$$

The impurity density N_I determines the Landau Level broadening $\Gamma=W_{\zeta\zeta'}(\varepsilon,\varepsilon')/\hbar$. Evaluating $W_{\zeta\zeta'}(\varepsilon,\varepsilon')/\hbar$ in the $u\to0$ limit without taking into account the SOI, we obtain $N_I\approx4\pi[(2\epsilon\epsilon_0/e^2)]^2\Gamma/\hbar$.

The Hall conductivity σ^{nd}_{xy} is given by

$$\sigma^{nd}_{xy}=\frac{2i\hbar e^2}{S_0}\sum_{\zeta,\zeta'}f(E_\zeta)[1-f(E'_\zeta)]\langle\zeta|v_x|\zeta'\rangle\times\langle\zeta'|v_y|\zeta\rangle\frac{1-e^{\beta(E_\zeta-E'_\zeta)}}{(E_\zeta-E'_\zeta)^2},\quad \zeta'\neq\zeta. \quad (18)$$

The evaluation of Eq. (18) proceeds along the lines of Ref. 25 using the the matrix elements $\langle\zeta|v_\mu|\zeta'\rangle$, $\mu=x,y$, given in the Appendix. Taking $\varepsilon^\sigma_{n+1}-\varepsilon^\sigma_n\approx\hbar\omega_c$, leads readily to

$$\sigma^{nd}_{xy}=\frac{e^2}{4\pi\hbar}\sum_{s=0}^{\infty}(s+1)[\mathcal{B}_s(f^+_s-f^+_{s+1})+\mathcal{C}_s(f^-_{s+1}-f^-_{s+2})], \quad (19)$$

where

$$\mathcal{B}_s=\frac{1}{\mathcal{A}_s^2\mathcal{A}_{s+1}^2}\left\{\Theta_s^2+\frac{2m^*\alpha\mathcal{D}_{s+1}}{\hbar^2\omega_c\sqrt{s+1}}\times\left[\frac{\alpha\mathcal{D}_{s+1}}{\hbar\sqrt{s+1}}+\left(\frac{\hbar}{m^*l_c}+\Theta_s\right)\Big/\sqrt{2}\right]\right\}, \quad (20)$$

$$\mathcal{C}_s=\frac{1}{\mathcal{A}_{s+1}^2\mathcal{A}_{s+2}^2}\left\{\Theta_s'^2+\frac{2m^*\alpha\mathcal{D}_{s+1}}{\hbar^2\omega_c\sqrt{s+1}}\times\left[\frac{\alpha\mathcal{D}_{s+1}}{\hbar\sqrt{s+1}}-\left(\frac{\hbar}{m^*l_c}+\Theta'_s\right)\Big/\sqrt{2}\right]\right\}; \quad (21)$$

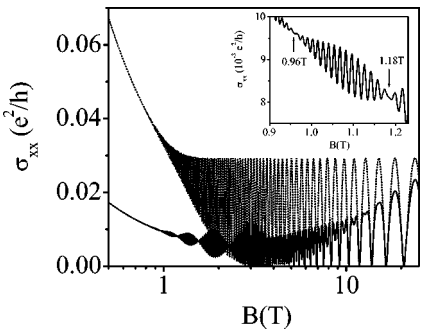

FIG. 2. Conductivity σ_{xx} as a function of the magnetic field B. The dotted curve is for $\alpha=0$ eV m and the solid one for $\alpha=1.2\times10^{-11}$ eV m. The inset shows the oscillations between the fourth and fifth node.

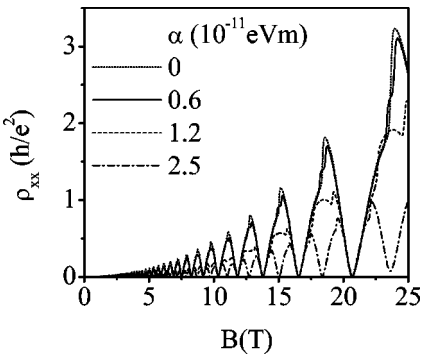

FIG. 3. The resistivity ρ_{xx} as a function of the magnetic field B for different values of the parameter α as indicated.

here $\Theta_s=1+[s/(s+1)]^{1/2}\mathcal{D}_s\mathcal{D}_{s+1}$ and $\Theta_s'=1+[(s+2)/(s+1)]^{1/2}\mathcal{D}_{s+1}\mathcal{D}_{s+2}$. We notice that if $\alpha=0$, we have $\Theta_s=\Theta_s'=\mathcal{A}_{s+1}=\mathcal{A}_{s+2}=1$ and Eq. (19) becomes $\sigma_{xy}^{nd}=(e^2/h)\Sigma_{s=0}^{\infty}f_s$, i.e., the conductivity expression pertinent to the integer quantum Hall effect.[25]

The resistivity tensor, $\rho_{\mu\nu}$ is given in terms of the conductivity tensor. We use the standard expressions $\rho_{xx}=\sigma_{yy}/S$, $\rho_{yy}=\sigma_{xx}/S$, $\rho_{yx}=\rho_{xy}=-\sigma_{yx}/S$, where $S=\sigma_{xx}\sigma_{yy}-\sigma_{xy}\sigma_{yx}$.

B. Numerical results

In the numerical evaluation of the conductivity we assume that the δ functions appearing in Eq. (16) are broadened and replace them with the Gaussian function $(1/\sqrt{2\pi}\Gamma)e^{-x^2/(2\Gamma^2)}$. Further, if not otherwise specified, we use the following parameters: $T=0.4$ K, $\Gamma=1.5$ meV, $g=0$, $m^*=0.05$, $N_e=4\times10^{16}$ m^{-2}. In Fig. 2 we plot $\sigma_{xx}^{\rm col}$ in the small u limit, see Eq. (16), as a function of the magnetic field. The dotted curve shows $\sigma_{xx}^{\rm col}$ in the absence of SOI and the solid one in its presence with $\alpha=1.2\times10^{-11}$ eV m. For low magnetic fields and weak α the conductivity decreases quickly with α and saturates around $\alpha=2\times10^{-11}$ eV m. The typical beating pattern appears when the subband broadening is of the same order as the Landau-level separation. At high magnetic fields, the effect of SOI is weakened and the beating pattern is replaced by split conductivity peaks. The latter approaches that without SOI when the magnetic field becomes very strong. One of the segments, with a typical beating pattern between the fourth and the fifth node, is shown in the inset. From Fig. 1 we see that the mth node is located near the nth Landau level when $E_{n+m}^{-}\simeq(E_{n-1}^{+}+E_n^{+})/2$. Using this expression for large n and small m ($n\gg1$), we can obtain the ratio of the Landau index over the magnetic field. The result is

$$\frac{n_m}{B_m}\simeq\frac{(2m-1)(2m+3)e\hbar^2+8gm^*\hbar e-4m^{*2}g^2\hbar^2e}{32m^{*2}\alpha^2}. \tag{22}$$

This leads to

$$\frac{n_{m+1}}{B_{m+1}}-\frac{n_m}{B_m}\simeq\frac{(m+1)\hbar^2e}{4m^*\alpha^2}. \tag{23}$$

If we keep the electron density N_e constant and use the definition of the filling factor $\nu=N_e2\pi l_c^2$, we can approximate B_m by $B_m=\pi\hbar N_e/en_m$, and obtain

$$\frac{1}{B_{m+1}^2}-\frac{1}{B_m^2}\simeq\frac{(m+1)\hbar e^2}{4\pi m^{*2}\alpha^2N_e} \tag{24}$$

and

$$n_{m+1}^2-n_m^2\simeq\frac{(m+1)\pi\hbar^3}{4m^{*2}\alpha^2}. \tag{25}$$

Equations (24) and (25) can be used to estimate the Rashba parameter α. For instance, using the inset of Fig. 2 provides $n_4=71$ and $n_5=87$. Experimentally, the SdH oscillations in the resistivity of a 2D system, in the presence of SOI, are usually viewed as resulting from a 2D system with two subbands[15,21] with the SOI splitting at the Fermi level $\Delta_R=2\alpha k_F$ serving as the subband separation. Following this line of reasoning, we can also analyze the results shown in the inset of Fig. 2. The SdH frequency difference between the plus and minus oscillations is $m\times B_m\simeq4.8$ T and corresponds to a carrier density difference $\Delta N=1.16\times10^{15}$ m^{-2}. This leads[18] to $\alpha=\hbar k_F\Delta N/(2m^*N_e)=1.1\times10^{-11}$ eV m.

In Fig. 3 we plot the resistivity ρ_{xx} for different strengths α as a function of the magnetic field. With the increase of α each resistivity peak becomes lower and gradually splits into two peaks. However, the shape of the gaps is not affected by SOI. We also notice that all peaks retain almost the same form after splitting.

Figure 4 shows the Hall resistivity ρ_{xy} versus the magnetic field B. For strong magnetic fields we see the integer quantum Hall effect plateaus at h/ne^2, where n is an integer. In the presence of SOI, one more plateau with value $2h/(2n+1)e^2$ appears between every two plateaus of order n and $n+1$. The size of this new plateau increases with α. It is worth noting that these extra plateaus require rather strong α and may easily shrink or disappear if disorder is included in the calculation of the Hall resistivity. In the lower inset of

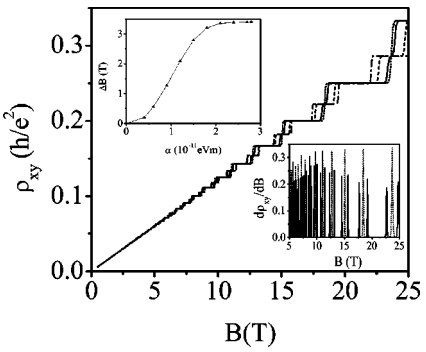

FIG. 4. Hall resistivity ρ_{xy} as a function of the magnetic field B. The different curves correspond to different α and are marked as in Fig. 3. The lower inset shows the derivative of ρ_{xy} with respect to B versus B for $\alpha=0$ (dotted curve) and $\alpha=1.2\times10^{-11}$ eV m (solid curve). In the upper inset the difference ΔB between the values of the two peaks in this derivative, into which the $\alpha=0$ peak near $B=24$ T splits, is shown as a function of α.

Fig. 4 we plot the derivative $d\rho_{xy}/dB$ as a function of B. Each peak, corresponding to a sharp jump of the resistivity, splits into two peaks which separate from each other, by a distance ΔB, with increasing α. The dependence of ΔB on α is plotted in the upper inset. The split increases slowly for small α and saturates at about $\alpha=2\times10^{-11}$ eV m.

C. Comparison with the experiment

In the following, we will analyze, using Eq. (24), two typical measurements of the SdH oscillation in InGaAs/InAlAs heterostructures, assuming the Rashba term dominates the contribution of the observed zero-field spin splitting. Reference 26 provides results for two samples A and C. For sample A, with effective mass $m^*=0.046$ and sheet density $n_s=1.75\times10^{12}$ cm^{-2}, the positions of the first six nodes are, respectively, at fields, $B_1=0.873$ T, $B_2=0.46$ T, $B_3=0.291$ T, $B_4=0.227$ T, $B_5=0.183$ T, $B_6=0.153$ T. From the positions of any two successive nodes B_m and B_{m+1}, we extract the Rashba parameter α. The results are shown as full triangles in Fig. 5; as shown α fluctuates and converges to the average value $\alpha=3.7\times10^{-12}$ eV m with increasing node number m. The consistency of the α values extracted from different nodes convinces us that the Rashba term is the main cause of the beating pattern here. It may be that bulk SOI contributes also and results in the variation of α when different nodes are used. The calculated spin splitting at the Fermi level is $\delta_F=2\alpha k_F=2.45$ meV and is the same as the extrapolated result from Ref. 26. The same analysis has been done for sample C, with $n_s=1.46\times10^{12}$ cm^{-2} and $B_1=0.65$ T, $B_2=0.312$ T, and $B_3=0.204$ T; the results are shown in Fig. 5 as squares. The zero-field spin splitting at the Fermi level is 1.7 meV and is close to the value 1.5 meV given in Ref. 26. In the inset of Fig. 5 we show the calculated diagonal resistivity for sample A of Ref. 26 at temperature $T=0.5$ K. A magnetic-field-dependent subband broadening is adopted, $\Gamma=\Gamma_0\sqrt{B}$, with $\Gamma_0=0.68$ meV/T$^{1/2}$. The second node is well fitted, while the

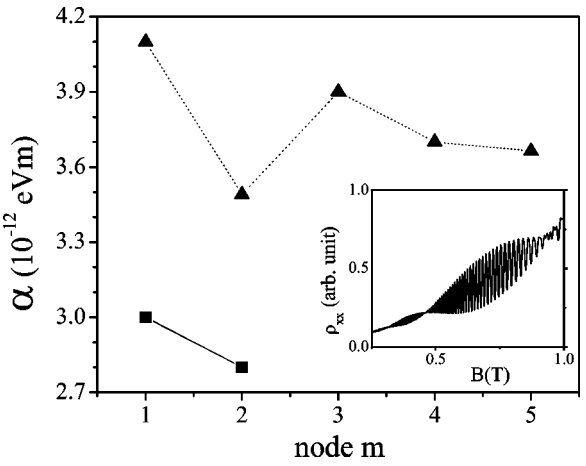

FIG. 5. Strength α of the Rashba term, as a function of the observed (Ref. 26) node number m, extracted from Eq. (24) and measured node positions B_m and B_{m+1} for sample A (triangles) and sample C (squares). The inset shows our calculated ρ vs B beating pattern for sample A. The dotted and solid lines are guides to the eye.

first node appears at a slightly higher magnetic field and 40 oscillations are enclosed between them whereas the number observed in Ref. 26 is 35.

In Ref. 15 the SdH oscillations of a 2DEG confined in a gate-controlled InGaAs layer were observed under different gate voltages V_g, at values -1, -0.7, -0.3, 0, 0.3, 0.5, and 1.5 V. The electron effective mass ranges from $m^*=0.049$, at $V_g=-1$ V, to $m^*=0.052$, at $V_g=1.5$ V, and the corresponding sheet density changes from $n=1.6$ to $n=2.41\times10^{12}$ cm^{-2}. The first nodes B_1 corresponding to the V_g values given above are at fields $B_1=2.032$, 2.025, 2.011, 1.98, 1.923, 1.894, 1.87 T, respectively, and the second nodes at $B_2=1.13$, 1.079, 1.035, 0.966, 0.915, 0.9, 0.871 T. Em-

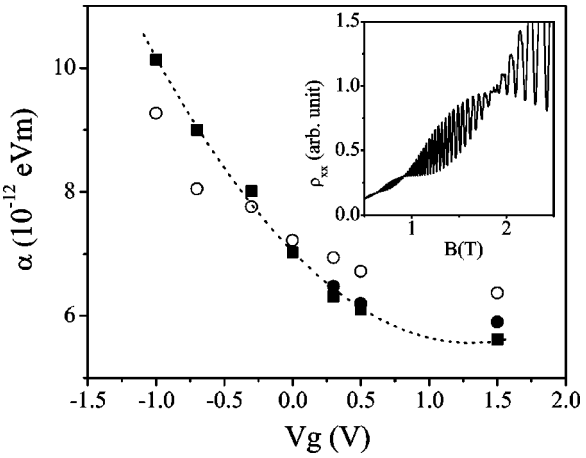

FIG. 6. Strength α of the Rashba term, as a function of the applied gate voltage, extracted from Eq. (24) (squares) and pertinent to the results of Ref. 15. The latter are shown by the open (solid) circles when the first (second) nodes are fitted as in Ref. 15. The inset shows our calculated ρ vs B beating pattern for $V_g=0.3$ V, $T=0.4$ K. The dotted curve, produced by $\alpha=7.04-2.26V_g+0.87V_g^2$, is a fit to our results (squares).

ploying Eq. (24) we evaluate the Rashba parameter as a function of the gate voltage. We show the results in Fig. 6 as filled squares and fit them with the dashed curve, obtained with $\alpha = 7.04 - 2.26V_g + 0.87V_g^2$. Our results are consistent with those given in Ref. 15 obtained by fitting the first nodes (open circles) of the observed beating pattern with those obtained from an approximate evaluation of the resistivity; the fitting of the second nodes is shown by the filled circles. Our calculated magnetoresistivity, as a function of the magnetic field, for $V_g = 0.3$ V and $T = 0.4$ K, is shown in the inset of Fig. 6. Here we find the second node is well fitted and a smaller number of oscillations ($n_2 - n_1 \simeq 26$) than that observed ($\simeq 28$). It is worth noting that the value of α we obtained, after analyzing these two examples for InAs-based heterostructures, is of the same order of magnitude as that found by the microscopic model proposed in Ref. 14 for comparable densities; from Fig. 3 of Ref. 14 the extracted value of α is $\simeq 2 \times 10^{-11}$ eV m at density $n_s = 10^{12}$ cm^{-2}.

Our way to extract the parameter α from the experimental SdH oscillations leads to theoretical results that are in rather good agreement with those obtained by fitting experimental curves. One advantage of Eq. (24) is that it is independent of the Zeeman splitting. Accordingly, the conclusion can be drawn that the Rashba effect plays the main role in the formation of beating patterns in the SdH oscillations in the measurements discussed above. However, as stated above some mismatches exist, e.g., the α value extracted from different node sets can vary and not all observed nodes can be fitted well with the same accuracy. Also, the measured dependence of the resistivity on the magnetic field is not well recovered by this simple model. This might be a result of the approximations introduced in it, e.g., the neglect of the bulk SOI in the model, the simplified impurity potential, the small u approximation or some unconsidered mechanism influencing the resistivity.

IV. CONCLUDING REMARKS

We studied magnetotransport in a 2D electron system in the presence of the Rashba spin-orbit interaction term. When the subband broadening is much smaller than the Landau level separation, the effect of this term on the conductivity is manifested as a splitting of the SdH peaks. For week magnetic fields, with a level broadening comparable to the Landau level separation, a beating pattern appears in the conductivity plot as a function of the magnetic field. By measuring the position of two successive nodes, we can estimate the strength α of the Rashba term. The theory is in reasonably good agreement with the available experimental observations for ρ_{xx}. In strong magnetic fields, where the integer quantum Hall effect is observed, a sufficiently strong α creates new plateaus between the integer plateaus in the Hall resistivity and splits the SdH peaks of ρ_{xx}.

ACKNOWLEDGMENTS

We thank Dr. W. Xu for helpful discussions. This work was supported by the Canadian NSERC Grant No. OGP0121756.

APPENDIX

The x and y components of the velocity operator read

$$v_x = \frac{\partial H}{\partial p_x} = \begin{bmatrix} -i\hbar\nabla_x/m^* - \omega_c y & i\alpha/\hbar \\ -i\alpha/\hbar & -i\hbar\nabla_x/m^* - \omega_c y \end{bmatrix}, \tag{A1}$$

$$v_y = \frac{\partial H}{\partial p_y} = \begin{bmatrix} -i\hbar\nabla_y/m^* & \alpha/\hbar \\ \alpha/\hbar & -i\hbar\nabla_y/m^* \end{bmatrix}. \tag{A2}$$

Setting $\mathcal{E}_s = \omega_c l_c[s^{1/2} + \mathcal{D}_s\mathcal{D}_{s+1}(s+1)^{1/2}]/\sqrt{2}$, $\mathcal{F}_s = \omega_c l_c[(s-1)^{1/2} + \mathcal{D}_s\mathcal{D}_{s-1}s^{1/2}]/\sqrt{2}$, $\mathcal{G}_s = \omega_c l_c[\mathcal{D}_{s+1}s^{1/2} - \mathcal{D}_s(s+1)^{1/2} - \sqrt{2}(\alpha/\hbar\omega_c l_c)\mathcal{D}_s\mathcal{D}_{s+1}]/\sqrt{2\mathcal{A}_s\mathcal{A}_{s+1}}$, and $\mathcal{H}_s = \omega_c l_c[\mathcal{D}_s s^{1/2} - \mathcal{D}_{s-1}(s-1)^{1/2} - \sqrt{2}\alpha/\hbar\omega_c l_c]/\sqrt{2\mathcal{A}_s\mathcal{A}_{s-1}}$, we can express the matrix elements of v_x and v_y in the Landau representation as follows:

$$\langle \Psi_s^-(k_x)|v_x|\Psi_{s'}^-(k_x')\rangle = -\frac{[\mathcal{E}_s - \alpha\mathcal{D}_s/\hbar]}{\sqrt{\mathcal{A}_s\mathcal{A}_{s+1}}}\delta_{s,s'-1}\delta_{k_x,k_x'} - \frac{[\mathcal{F}_s - \alpha\mathcal{D}_{s-1}/\hbar]}{\sqrt{\mathcal{A}_s\mathcal{A}_{s-1}}}\delta_{s,s'+1}\delta_{k_x,k_x'}, \tag{A3}$$

$$\langle \Psi_s^-(k_x)|v_y|\Psi_{s'}^-(k_x')\rangle = -\frac{i[\mathcal{E}_s - \alpha\mathcal{D}_s/\hbar]}{\sqrt{\mathcal{A}_s\mathcal{A}_{s+1}}}\delta_{s,s'-1}\delta_{k_x,k_x'} + \frac{i[F_s - \alpha\mathcal{D}_{s-1}/\hbar]}{\sqrt{\mathcal{A}_s\mathcal{A}_{s-1}}}\delta_{s,s'+1}\delta_{k_x,k_x'}, \tag{A4}$$

$$\langle \Psi_s^+(k_x)|v_x|\Psi_{s'}^+(k_x')\rangle = \langle \Psi_s^-(k_x)|v_y|\Psi_{s'}^-(k_x')\rangle|_{\alpha\to-\alpha}, \tag{A5}$$

$$\langle \Psi_s^+(k_x)|v_y|\Psi_{s'}^+(k_x')\rangle = \langle \Psi_s^-(k_x)|v_y|\Psi_{s'}^-(k_x')\rangle|_{\alpha\to-\alpha}, \tag{A6}$$

$$\langle \Psi_s^-(k_x)|v_x|\Psi_{s'}^+(k_x')\rangle = i\mathcal{G}_s\delta_{s,s'-1}\delta_{k_x,k_x'} - i\mathcal{H}_s\delta_{s,s'+1}\delta_{k_x,k_x'}, \tag{A7}$$

$$\langle \Psi_s^-(k_x)|v_y|\Psi_{s'}^+(k_x')\rangle = -\mathcal{G}_s\delta_{s,s'-1}\delta_{k_x,k_x'} - \mathcal{H}_s\delta_{s,s'+1}\delta_{k_x,k_x'}. \tag{A8}$$

The matrix elements of the position operator in the y direction are

$$\langle \Psi_s^-(k_x)|y|\Psi_{s'}^-(k_x')\rangle$$

$$= \frac{l_c}{\sqrt{2\mathcal{A}_s\mathcal{A}_{s+1}}}[s^{1/2}+(s+1)^{1/2})\mathcal{D}_s\mathcal{D}_{s+1}]\delta_{s,s'-1}\delta_{k_x,k_x'}$$

$$+ \frac{l_c}{\sqrt{2\mathcal{A}_s\mathcal{A}_{s-1}}}[(s-1)^{1/2}+s^{1/2}\mathcal{D}_s\mathcal{D}_{s-1}]\delta_{s,s'+1}\delta_{k_x,k_x'}$$

$$+ y_c\delta_{s,s'}\delta_{k_x,k_x'} \tag{A9}$$

$$\langle \Psi_s^+(k_x)|y|\Psi_{s'}^+(k_x')\rangle$$

$$= \frac{l_c}{\sqrt{2\mathcal{A}_s\mathcal{A}_{s+1}}}[\mathcal{D}_s\mathcal{D}_{s+1}s^{1/2}+(s+1)^{1/2}]\delta_{s,s'-1}\delta_{k_x,k_x'}$$

$$+ \frac{l_c}{\sqrt{2\mathcal{A}_s\mathcal{A}_{s-1}}}[\mathcal{D}_s\mathcal{D}_{s-1}(s-1)^{1/2}+s^{1/2}]\delta_{s,s'+1}\delta_{k_x,k_x'}$$

$$+ y_c\delta_{s,s'}\delta_{k_x,k_x'}. \tag{A10}$$

The form factors $|F_{\zeta\zeta'}(u)|^2$ read

$$|F^-_{s,k_x;s',k_x'}(u)|^2 = |\langle \Psi_s^-(k_x)|e^{i\vec{q}\cdot\vec{r}}|\Psi_{s'}^-(k_x')\rangle|^2$$

$$= [(s'/s)^{1/2}L_{s-1}^{s'-s}(u)+\mathcal{D}_m\mathcal{D}_{m'}L_s^{s'-s}(u)]^2$$

$$\times \frac{s!}{s'!}\frac{u^{s'-s}}{\mathcal{A}_s\mathcal{A}_{s'}}e^{-u}\delta_{k_x,k_x'+q_x}, \tag{A11}$$

$$|F^+_{s,k_x;s',k_x'}(u)|^2 = |\langle \Psi_s^+(k_x)|e^{i\vec{q}\cdot\vec{r}}|\Psi_{s'}^+(k_x')\rangle|^2$$

$$= [(s'/s)^{1/2}\mathcal{D}_m\mathcal{D}_{m'}L_{s-1}^{s'-s}(u)$$

$$+ L_s^{s'-s}(u)]^2\frac{s!}{s'!}\frac{u^{s'-s}}{\mathcal{A}_s\mathcal{A}_{s'}}e^{-u}\delta_{k_x,k_x'+q_x}. \tag{A12}$$

[1] S. Datta and B. Das, Appl. Phys. Lett. **56**, 665 (1990).
[2] X. F. Wang, P. Vasilopoulos, and F. M. Peeters, Phys. Rev. B **65**, 165217 (2002).
[3] E. Tutuc, E. P. De Poortere, S. J. Papadakis, and M. Shayegan, Phys. Rev. Lett. **86**, 2858 (2001); S. J. Papadakis *et al.*, Science **283**, 2056 (1999).
[4] J. P. Lu, J. B. Yau, S. P. Shukla, M. Shayegan, L. Wissinger, U. Rossler, and R. Winkler, Phys. Rev. Lett. **81**, 1282 (1998).
[5] A. F. Morpurgo, J. P. Heida, T. M. Klapwijk, and B. J. van Wees, and G. Borghs, Phys. Rev. Lett. **80**, 1050 (1998).
[6] S. D. Ganichev, E. L. Ivchenko, V. V. Bel'kov, S. A. Tarasenko, M. Sollinger, D. Weiss, W. Wegscheider, and W. Prettl, Nature (London) **417**, 153 (2002).
[7] G. Dresselhaus, Phys. Rev. **100**, 580 (1955).
[8] E. I. Rashba and V. I. Sheka, Dokl. Akad. Nauk SSSR **2**, 162 (1959); E. I. Rashba, Sov. Phys. Solid State **2**, 1109 (1960).
[9] H. L. Stormer and Z. Schlesinger, A. Chang, D. C. Tsui, A. C. Gossard, and W. Wiegmann, Phys. Rev. Lett. **51**, 126 (1983).
[10] D. Stein, K. v. Klitzing, and G. Weimann, Phys. Rev. Lett. **51**, 130 (1983).
[11] Y. A. Bychkov and E. I. Rashba, J. Phys. C **17**, 6039 (1984).
[12] G. Lommer, F. Malcher, and U. Rössler, Phys. Rev. B **32**, 6965 (1985); Phys. Rev. Lett. **60**, 728 (1988).
[13] J. Luo, H. Munekata, F. F. Fang, and P. J. Stiles, Phys. Rev. B **38**, 10 142 (1988); **41**, 7685 (1990).
[14] E. A. de Andrada e Silva, G. C. La Rocca, and F. Bassani, Phys. Rev. B **50**, 8523 (1994).
[15] J. Nitta, T. Akazaki, H. Takayanagi, and T. Enoki, Phys. Rev. Lett. **78**, 1335 (1997); C. M. Hu, J. Nitta, T. Akazaki, H. Takayanagi, J. Osaka, P. Pfeffer, and W. Zawadzki, Phys. Rev. B **60**, 7736 (1999).
[16] G. Engels, L. Lange, Th. Schäpers, and H. Lüth, Phys. Rev. B **55**, R1958 (1997).
[17] D. Grundler, Phys. Rev. Lett. **84**, 6074 (2000).
[18] J. P. Heida, B. J. van Wees, J. J. Kuipers, T. M. Klapwijk, and G. Borghs, Phys. Rev. B **57**, 11 911 (1998).
[19] L. W. Molenkamp, G. Schmidt, and G. E. W. Bauer, Phys. Rev. B **64**, R121202 (2001).
[20] T. Koga, J. Nitta, T. Akazaki, and H. Takayanagi, Phys. Rev. Lett. **89**, 046801 (2002).
[21] K. Tsubaki, N. Maeda, T. Saitoh, and N. Kobayashi (unpublished).
[22] T. Englert, D. Tsui, A. Gossard, and C. Uihlein, Surf. Sci. **113**, 295 (1982).
[23] P. Vasilopoulos and C. M. Van Vliet, J. Math. Phys. **25**, 1391 (1984).
[24] P. Vasilopoulos and C. M. Van Vliet, Phys. Rev. B **34**, 1057 (1986).
[25] P. Vasilopoulos, Phys. Rev. B **32**, 771 (1985).
[26] B. Das, D. C. Miller, S. Datta, R. Reifenberger, W. P. Hong, P. K. Bhattacharya, J. Singh, and M. Jaffe, Phys. Rev. B **39**, 1411 (1989).